# GT2019-91079

# THE EFFECTS OF EXIT BOUNDARY CONDITION ON PRECESSING VORTEX CORE DYNAMICS

Danielle Mason, Sean Clees<sup>1</sup>, Mark Frederick<sup>2</sup>, Jacqueline O'Connor

Pennsylvania State University University Park, PA, United States

#### **ABSTRACT**

Many industrial combustion systems, especially power generation gas turbines, use fuel-lean combustion to reduce NO<sub>x</sub> emissions. However, these systems are highly susceptible to combustion instability, the coupling between combustor acoustics and heat release rate oscillations of the flame. It has been shown in previous work by the authors that a precessing vortex core (PVC) can suppress shear layer receptivity to external perturbations, reducing the potential for thermoacoustic coupling. The goal of this study is to understand the effect of combustor exit boundary condition on the flow structure of a swirling jet to increase fundamental understanding of how combustor design impacts PVC dynamics. The swirling jet is generated with a radial-entry, variable-angle swirler, and a quartz cylinder is fixed on the dump plane for confinement. Combustor exit constriction plates of different diameters are used to determine the impact of exit boundary condition on the flow field. Particle image velocimetry (PIV) is used to capture the velocity field inside the combustor. Spectral proper orthogonal decomposition, a frequency-resolved eigenvalue decomposition that can identify energetic structures in the flow, is implemented to identify the PVC at each condition in both energy and frequency space. We find that exit boundary diameter affects both the structure of the flow and the dynamics of the PVC. Higher levels of constriction (smaller diameters) force the downstream stagnation point of the vortex breakdown bubble upstream, resulting in greater divergence of the swirling jet. Further, as the exit diameter decreases, the PVC becomes less energetic and less spatially defined. Despite these changes in the base flow and PVC coherence, the PVC frequency is not altered by the exit boundary constriction. These trends will help inform our understanding of the impact of boundary conditions on both static and dynamic flame stability.

## **NOMENCLATURE**

	L J
S	Swirl number
r	Radial coordinate [m]
x	Downstream coordinate [m]
ISL	Inner shear layer
PIV	Particle image velocimetry
PVC	Precessing vortex core
RMS	Root mean squared
SLM	Standard liters per minute
SPOD	Spectral proper orthogonal decomposition
SNR	Signal to noise ratio

Nozzle diameter [m]

Vortex breakdown

#### INTRODUCTION

VB

Many industrial combustion systems, especially power generation gas turbines, use fuel-lean combustion to reduce  $NO_x$  emissions. However, these systems are highly susceptible to both static and dynamic combustion stability issues. Static stability can be compromised when the flame propagation speed, which decreases at the low equivalence ratios required for  $NO_x$  abatement, is too low to achieve continuous flame-holding in the high-velocity stream of the combustor [1]. Dynamic stability, often referred to simply as "combustion instability," is also an issue at these conditions as the flame is highly susceptible to mixture perturbations [2]. Combustion instabilities are driven by coupling between combustor acoustics and heat release rate oscillations [3]. This coupling can cause increased emissions, lower engine operability, and, in severe cases, engine failure.

If the system surpasses the "static" stability limit, blow-off can occur. Flame stabilization is typically ensured by creating a recirculation zone along the center line of the combustor that promotes mixing and feeds hot, radical-filled gases to the base of the flame. Swirling flows with vortex breakdown (VB) are the

<sup>&</sup>lt;sup>1</sup> Current affiliation: Mechanical Engineering, Stanford University

<sup>&</sup>lt;sup>2</sup> Current affiliation: Aeronautics and Astronautics, Purdue University

standard structure used to create this recirculation, which provides improved mixing compared to other designs with recirculation, such as bluff bodies.

The structure of a swirling flow varies with swirl number [4], which is defined as the ratio of axial flux of angular momentum to axial flux of axial momentum [5]. There are typically two main bifurcations in the structure and stability of swirling flows. The first critical swirl number is at the occurrence of vortex breakdown. The second critical swirl number signals the presence of a precessing vortex core (PVC). A PVC is a helical structure that causes the vortex breakdown bubble to precess about the nozzle axis. These critical numbers vary by experiment setup, but from previous work on a free jet using the same experimental facility, the critical swirl numbers for vortex breakdown and PVC onset in this experiment are S=0.56 and S=0.73, respectively [6]. Typically, the PVC is the most energetic motion in the flow and is characterized by a periodic helical motion whose frequency increases with increasing swirl number [7].

Confinement of a swirling jet can significantly alter the structure of the flow field. Mathews  $et\ al.$  [8] performed preliminary experiments of confined, non-reacting flow in the experimental configuration used in this study, shown in Figure 1. They showed that confinement introduces corner recirculation zones and decreases the axial velocity at all radial positions for all swirl numbers tested (S=0.18, 0.79, and 1.43). For low swirl numbers, the shear layers thicken and the flow spreads radially more rapidly as a function of downstream distance. For high swirl numbers, the vortex breakdown bubble is larger with confinement and the location where the swirling jet impacts the wall is closer to the nozzle exit [7].

Geometry of the combustion chamber plays a large role in the flow field formation, particularly in swirling flows. The exit radius of the combustion chamber has a large impact on the flow field, as variations in the exit radius change the pressure profile in the combustions chamber. Syred  $et\ al.$  [7] studied the effect of exit diameter size on swirling flow structure. In this study, they increased the ratio of exit radius to combustion chamber radius from S=0.5 to 0.63 and at two swirl number (S=0.99 and 1.63) for the application of industrial boilers. The decrease of the exit radius increased recirculation size and decreased the peak axial velocity at both swirl numbers.

These observations align with work by Darmofal [9] on vortex breakdown in tubes, where he showed that adding an adverse pressure gradient could change the critical swirl number for vortex breakdown and the structure of the vortex breakdown bubble at a given swirl number. The reason for these changes is attributed to the "criticality" of the flow, or the ability for disturbances to travel both upstream and downstream in the flow field. This theory, used in work by Darmofal and coworkers [10], [11], Leibovich and coworkers [12], [13], and Benjamin [14], clearly connects the downstream boundary condition with the behavior of the vortex breakdown region. Work by Escudier and Keller [15] also provided experimental substantiation of these theoretical predictions by looking at the "recovery" of the flow after vortex breakdown. Though the language of flow criticality

is not used in modern flow stability studies, theoretical work by Healey [16] showed that these ideas are analogous to the inviscid linear stability theory that is commonly used to predict both the onset of vortex breakdown [17,18] and the appearance of precessing vortex cores [19,20].

In this study, we are particularly interested in the impact that confinement and exit boundary condition have on the structure of the flow and the dynamics of the precessing vortex core. Our previous work [8] showed that confinement changed the structure as well as the receptivity of the shear layer to longitudinal excitation, but the work was preliminary and only considered a limited number of swirl numbers. More recent work in unconfined swirling jets has shown that the existence of a precessing core can suppress the receptivity of the shear layer to external perturbations, reducing the likelihood of thermoacoustic coupling in velocity-coupled systems [6]. Linear stability analysis by Manoharan and Hemchandra [19] showed that suppression of the shear layer receptivity is driven by shear layer thickening, which is an effect of the precessing vortex core. It was shown experimentally and in theory that the growth rate of disturbances in the shear layer of swirling flows with PVCs is much smaller than flows without this instability.

The goal of this work is to understand the impact of confinement and exit boundary condition on the structure and dynamics of the precessing vortex core in this swirl-stabilized combustor. Given that the structure of the vortex breakdown bubble is expected to change with changes to the exit boundary condition, we expect that these changes in flow structure will impact the PVC dynamics. As the PVC could be a potentially effective way of suppressing velocity-coupled combustion instability in swirl-stabilized flames, a better parametric understanding of the impact of combustor geometry on this structure will aid in the design of thermoacoustically-resistant combustors. In this work, we have found that the PVC is present at a large range of swirl numbers and boundary conditions, but that severe restrictions of the combustor exit can suppress the PVC, reducing its efficacy for instability suppression.

The remainder of the paper is organized as follows. We provide a brief overview of the experimental configuration, which has been discussed in much more detail in Refs. [6,8,21], and introduce the analysis methods used to quantify the dynamics of the PVC. Next, we discuss the impact of confinement and exit boundary conditions on the time-averaged structure of the flow, and then on the PVC dynamics. Changes to the PVC dynamics are linked back to the base flow and we hypothesize the reasons for changes to the PVC based on our previous linear stability analyses in unconfined flows. Finally, we conclude by discussing the impact of these results on design of stable combustion systems.

#### **EXPERIMENTAL CONFIGURATION**

Seen in Figure 1, the experimental facility used in this study is the same as used in Mathews *et al.* [8] and Fredrick *et al.* [6]. There are three main components of the facility. The first component is an injector nozzle with two pressure transducers to measure pressure fluctuations. The second section is the swirler

chamber with a radial entry, variable-angle swirler, and the third is the settling chamber with speakers for acoustic forcing of the system. A quartz cylinder is fixed on the dump plane for confinement analysis. Exit boundary condition constrictions of 1 in., 2 in., 3 in., and 4 in. diameters are used to determine the impact of exit boundary condition on the flow field.

Pressure transducers are located 1.84 cm and 6.92 cm upstream of the nozzle exit. A digital data acquisition system controls the pressure data and swirler angle. The pressure data is recorded at 20 kHz for a 3 second duration. The swirler is moved by a stepper motor attached to the base of the experiment. The blades of the swirler can range from -70° to 70° with a 2.5° resolution. In this experiment, the swirler is varied from 40° to 70° in steps of 2.5°. The bulk flow velocity is 28 m/s (953 SLM with a maximum variance of 3 SLM).

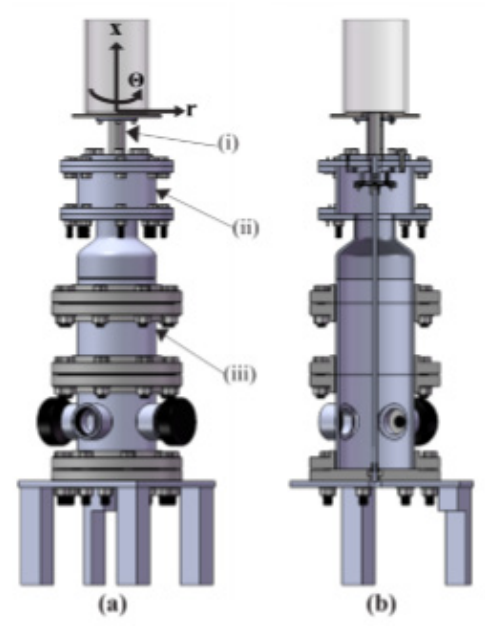


Figure 1. Experimental facility.

# **Diagnostics**

Particle image velocimetry (PIV) was used to calculate the velocity field inside the quartz chamber. Images of the field were captured by two high speed cameras (SA5 Photron CMOS high speed cameras with 50 mm lenses) in a forward-forward scattering stereo-imaging set up. The images were captured in the *x-r* plane, as defined by the coordinate system in Figure 1. A Hawk/Darwin Duo Nd-YAG, 532 nm wavelength, 60 W laser is used for PIV along with 1-2 micron aluminum oxide particles that can trace flow oscillations up to 4000 Hz. The thickness of the laser sheet was approximately 1 mm. The field of view was 3 in. high and 3 in. wide with a vector field resolution of one vector every 1.26 millimeters.

The images were sampled at 5 kHz with an interframe time ranging from 21 to 23 microseconds depending on swirl angle. The duration of recording was one second, producing 5000 images per test case. Velocity vectors are calculated in DaVis 8.3.1 with a sub-over time Gaussian filter to subtract out the

reflections of the quartz glass combustor liner. Cross-correlation with multi-pass iterations with decreasing window sizes is used. The first pass is a 32x32 pixel interrogation window with a 50% overlap followed by 2 passes with a 16x16 pixel interrogation with a 50% overlap. If the vector is more than 3 times the RMS of the surrounding vectors, the vector is removed and replaced. Additionally, universal outlier detection removes and replaces spurious vector results. The resulting uncertainty in the instantaneous velocity vectors, calculated using DaVis, varies spatially over the velocity field, but within the jet the average velocity uncertainty is 1.13 m/s with a variance of 0.45 m/s.

#### Data Analysis

Spectral proper orthogonal decomposition (SPOD), a frequency resolved eigenvalue decomposition that can identify energetic structures in the flow, is implemented to find the most energetic motions and their mode shape in the fluctuating flow field. The SPOD methodology follows that of Towne et al. [22] and is used to identify the mode shape of the PVC as well as its frequency and amplitude of oscillation. We use SPOD rather than using snapshot POD, which provides spatially-orthogonal, energy-ordered modes of the dataset, because POD does not discern motions based on their spatiotemporal evolution, just their spatial correlations. As a result, tonal but spatially uncorrelated or low-energy oscillations are not necessarily separated from other motions in the POD, but can be identified in the SPOD. SPOD achieves this by calculating the eigenvalue problem on the cross-spectral density tensor, which results in spatial modes analogous to snapshot POD, but also provides frequency-resolved energy information about each mode.

#### **RESULTS**

The text matrix consisted of nine swirl numbers and four exit boundary conditions at one flow velocity. Table 1 provides an overview of the operating conditions of the tests performed in this study. The range of swirl numbers was chosen such that a PVC was present in the unconfined jet cases with the same swirler angle [6]. Here, we define swirl number based on the geometric swirl number definition [5], and so the swirl number is only based on the premixing hardware geometry, which did not change between the unconfined and confined tests. However, the actual level of swirl and the development of the flow field change significantly when confinement is added, which is discussed in the next sub-section.

Table 1. Experimental operating conditions.

Bulk flow velocity	28 m/s
Inlet temperature	73 °C
Geometric swirl numbers	0.39, 0.47, 0.56, 0.67, 0.79,
	0.95, 1.15, 1.43, 1.83
Combustor inlet diameter	1 in.
Dump ratio	15
Combustor exit diameter	1, 2, 3, 4 in.
Combustor exit area ratio	15, 3.75, 1.67, 1

#### Effect of exit boundary condition on time-averaged flow

Figure 2 shows the time-averaged velocity profiles over the range of swirl numbers and exit diameters tested. The colorbar indicates the time-averaged axial velocity and streamlines are provided in white to show the time-averaged structure of the flow. In this figure, three of the nine swirl numbers (in the rows) are chosen to represent important regimes of the flow field with swirl number and all four exit boundary diameter cases (in the columns) are shown for these swirl numbers.

The unconfined jet, not shown here but discussed in detail in Frederick *et al.* [6] and Clees *et al.* [21], undergoes a range of structures as the swirl number increases. At a swirl number of S=0.56, steady recirculation occurs at the centerline of the jet as a result of vortex breakdown. A weak PVC appears at S=0.79, where the PVC frequency and amplitude are variable in time due to the weakness of the instability; more discussion of this weak PVC can be found in Karmarkar *et al.* [23]. At swirl numbers above S=0.95, the PVC frequency and amplitude increase as the strength of recirculation along the centerline increases and the vortex breakdown bubble shifts upstream towards the nozzle.

The same progression of flow structure occurs in the confined flow case with the largest exit diameter, as shown in the fourth column in Figure 2. Here, a time-averaged central recirculation is seen at a swirl number of S=0.79, and the strength of recirculation increases as the swirl number increases. Additionally, the vortex breakdown bubble shifts upstream and grows wider, causing the annular jet around the bubble to deflect further towards the wall. This deflection causes the corner recirculation zone to increase in strength as well. The deflection of the annular jet is greater in the cases with confinement than in the free-jet case as a result of the corner recirculation zone; this

zone does not exist in the unconfined jet and so jet deflection is only controlled by the vortex breakdown bubble size and centrifugal forces on the swirling flow.

As the exit boundary diameter decreases, the progression of the time-averaged flow structure as a function of swirl number changes in several important ways. At a swirl number of S=1.15 in the 1 in. and 2 in. exit diameter cases, the effect of the constrained boundary condition appears in the field of view near x/D=3. Here, an acceleration of the flow exists along the centerline, which begins to affect the shape of the VB bubble, particularly at its downstream edge. This is likely due to the accelerating jet that is created near the exit of the combustor. This acceleration results in a lower overall recirculation strength along the centerline and slightly less deflection of the annular jets towards the walls.

At *S*=1.43 and 1.83 (shown in Figure 2), however, the effect of the downstream boundary condition varies for different levels of exit constriction. In the 1 in. case, the acceleration region downstream of the VB bubble shifts upstream, further deforming the VB bubble. However, in both the 3 in. and 2 in. cases, the centerline recirculation zone is elongated, opposite of what occurs in the 1 in. case, extending as a "neck" downstream of the VB bubble. It is unclear what effect at the exit boundary is causing this elongation of the velocity deficit zone, but similar flow structures have been seen in other swirl combustors with exit constriction [24].

Given that the strength of recirculation and the shear layer profiles drive the shape of the base flow upon which the PVC disturbance grows [19], it is expected that the PVC dynamics would be affected by these changes in the exit boundary condition. In particular, the PVC frequency and growth rate have

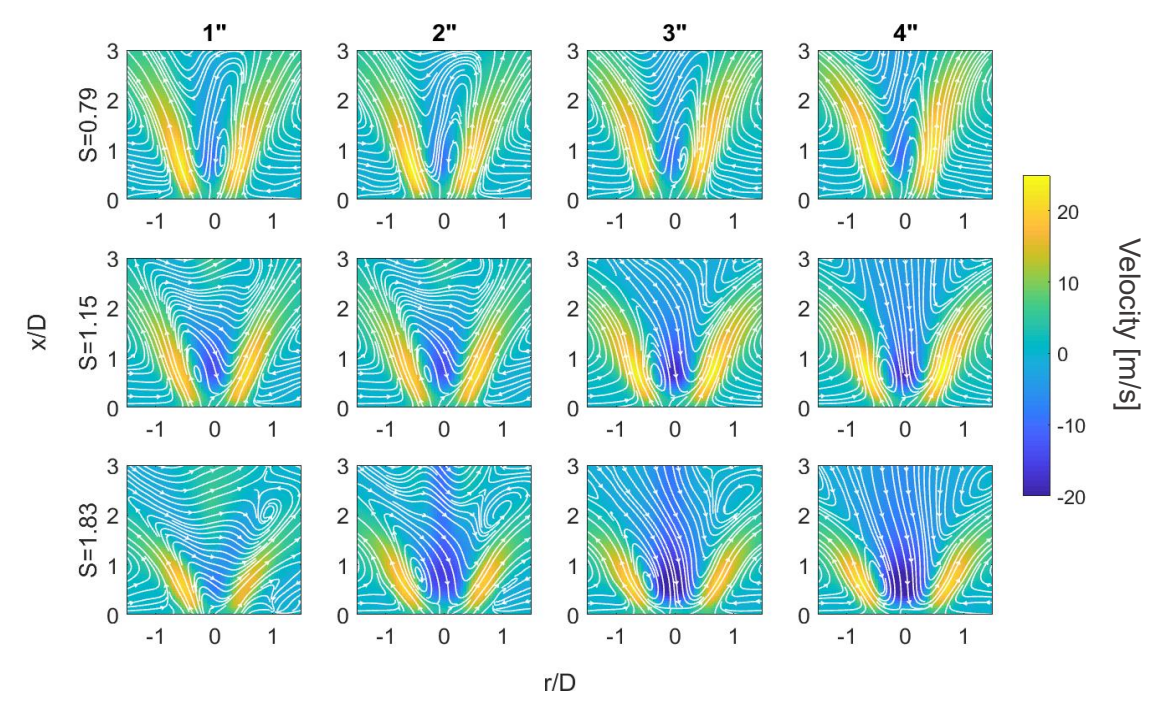


Figure 2. Time-averaged axial velocities of 0.79, 1.15, and 1.83 swirl numbers at four different exit diameters

been shown to be a function of the recirculation strength, shear layer thickness, and swirl number in the combustor in both local stability analyses [19,20] and global [25] stability analyses. As the structure of the recirculation zone, in particular, is altered by the presence of exit boundary constriction, we would expect that the dynamics of the PVC would be significantly altered.

#### Effect of exit boundary condition on PVC dynamics

A combination of pressure measurements in the swirler nozzle and SPOD of the high-speed, three-component velocity field were used to identify the frequency and amplitude of the PVC over a range of swirl numbers and exit boundary conditions. Figure 3 shows the Strouhal number, based on bulk flow velocity and jet diameter, of the PVC oscillation as a function of swirl number for the four exit boundary conditions as measured by both the pressure transducers and the SPOD; the pressure transducer data have a finer frequency resolution than the SPOD, but the frequencies of the two measurements align closely. The frequency of the PVC ranges from approximately 650 to 1100 Hz over this range of swirl numbers. As the PVC is relatively week at swirl numbers of S=0.56 and 0.79, the oscillations do not register on the pressure transducer and so no frequency data are reported from the pressure measurements at these conditions. The peak in the mode 1 spectrum of the SPOD is still quite distinctive at these conditions, though, and so those results are reported from the velocity data.

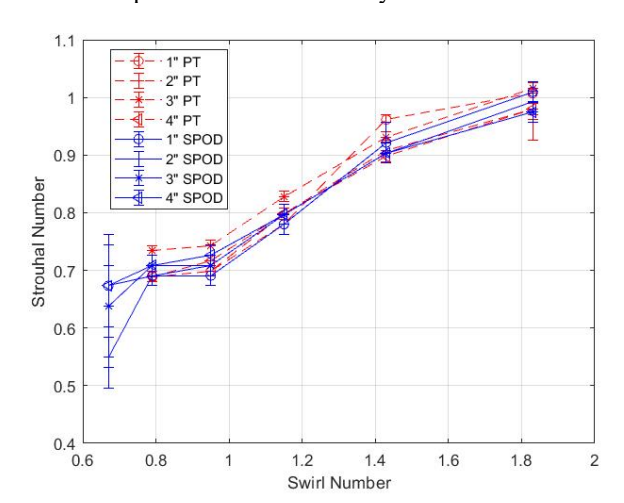


Figure 3. Strouhal number as a function of swirl number from pressure measurements and SPOD.

As in the unconfined jet, the frequency of the PVC increases with increasing swirl number. Surprisingly, the PVC frequency is rather insensitive to the exit boundary condition at each swirl number, with a variation of only a few tens of Hertz between conditions despite significant differences in the base flow. The uncertainty bars on the frequencies are calculated based on the full-width-half-max of the peak in the spectrum for each of the cases. This spectral variability is the result of jitter in the PVC spatiotemporal dynamics [23] and can be used as an indication of whether one frequency is significantly different from another at a different condition. The bars are larger at the lower swirl

numbers, particularly at S=0.67, where the PVC is quite weak and the frequency drifts significantly.

The amplitude of the PVC oscillation is shown in Figure 4, where the amplitude is quantified as the value of mode 1 at the PVC frequency from the SPOD of the three-component velocity field. Each mode's spectrum is calculated from an eigenvalue decomposition of the cross-spectral density of the different ensembles in the data, which is representative of a frequency-resolved turbulent kinetic energy. More details of the decomposition are provided in Towne *et al.* [22]. Analysis of the higher modes (modes 2 and above) shows much less coherent motion at the PVC frequency for all cases; as such, the PVC amplitude is calculated using the highest energy mode only.

While the frequency of the PVC is relatively insensitive to the exit boundary condition, the amplitude of the oscillation is highly sensitive to variations in the exit diameter. Figure 4 shows the amplitude of the PVC as a function of exit diameter for the full range of swirl numbers tested, and the impact of the exit boundary condition depends on the strength of the PVC. At lower swirl numbers (*S*=0.67, 0.79), the PVC amplitude increases slightly as the exit boundary diameter is decreased. At the larger exit diameters, the PVCs at these swirl numbers are relatively weak and influenced by a high amount of jitter, quantified by the width of the PVC spectral peak in the SPOD, as shown by the error bars in Figure 3. The increase in exit diameter reduces this jitter, reducing the width of the peak in the spectrum, which correlates with a strengthening of the PVC at its main frequency.

At the mid-range swirl number, S=0.95, the PVC amplitude is relatively insensitive to exit boundary condition and there is a lot of variation from case to case, an indication of a possible bifurcation in the behavior of the flow field at this condition. At the higher swirl numbers (S=1.15, 1.43, 1.83), the strength of the PVC weakens significantly as the exit diameter decreases (or the level of constriction increases).

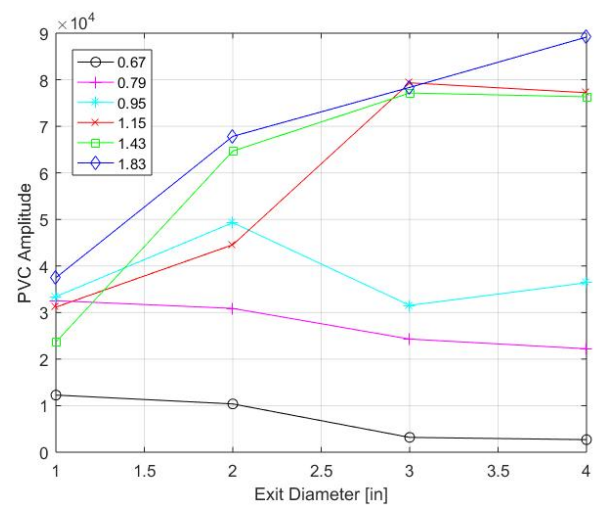


Figure 4. PVC amplitude vs. exit diameter from the SPOD for all swirl numbers

The strength of the PVC peak relative to the turbulent motion of the flow field is quantified as a signal to noise ratio

(SNR) of the SPOD peaks from mode 1 in Figure 5. The SNR trends closely follow those of the amplitude trends, showing that although the strength of the PVC varies with changes in swirl number and exit boundary condition, all the PVC modes identified in this analysis were coherent motions that oscillated with a significant amplitude relative to the background oscillations except at the lowest swirl number. This is a particularly important comparison at both the low and high swirl number conditions. At lower swirl numbers, the strength and coherence of the PVC is lower, as evidenced by both the amplitude and the full-width half-max of the peak in the mode 1 spectrum, and so the impact of turbulence on the dynamics of the PVC may be significant. At the higher swirl numbers, the PVC strength is significantly greater, but the turbulence level in the flow field has increased as the mean shear also increases due to the higher level of swirl. This can be quantified by the denominator of the SNR metric (not shown here), which increases as the swirl number increases. Despite this increase in turbulence intensity, the PVC motions remain significantly stronger than the incoherent oscillations in the background, as evidenced by the higher SNR values at higher swirl numbers.

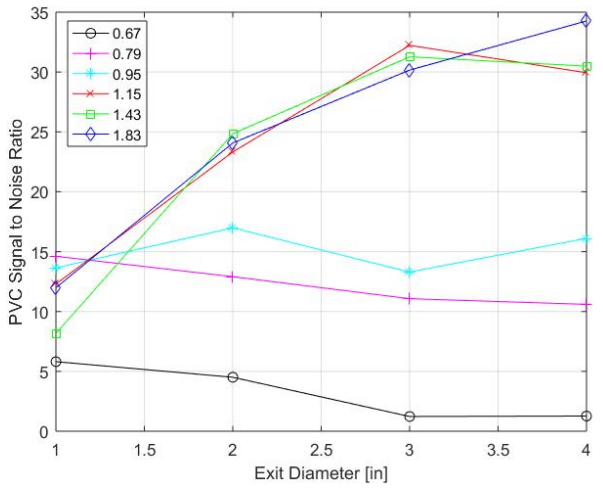


Figure 5. Signal to noise ratio of the PVC peak from the mode 1 spectra of the SPOD.

The difference in the effect of constriction with swirl number is likely the result of the different impact that the exit boundary condition has on the base flow. Work on precessing vortex core instabilities has shown that the presence of the precessing vortex core, as well as its frequency and growth rate, are a strong function of the level of swirl and the strength of the mean shear (or vorticity) in the inner shear layer around the vortex breakdown bubble [19]. At lower swirl numbers, the vortex breakdown bubble structure and recirculation strength are relatively insensitive to the exit boundary condition, as shown in the top row of Figure 2. However, as the swirl number increases and the strength of the vortex breakdown bubble increases, the exit boundary condition tends to have two different effects on the vortex breakdown structure. At swirl numbers below S=1.43, the "jetting" appears at small exit diameters, and above S=1.43, the

elongation of the vortex breakdown bubble occurs at large exit diameters.

These differences in VB bubble structure drive differences in the mean shear in the inner shear layer. Figure 6 and Figure 7 show time-averaged vorticity magnitude in the inner shear layer for the 4 in. and 1 in. cases, respectively. The vorticity is out-of-plane vorticity, calculated as the curl of the velocity field in the axial and radial directions. Work by Manoharan *et al.* [19] showed that the dynamics of the PVC, including its frequency and growth rate, were most sensitive to the level of swirl and the strength of the inner shear layer. We rely on this theoretical finding to help explain the trends in PVC amplitude with exit boundary diameter, assuming that increases in growth rate of the instability are indicative of the increasing "strength" (or amplitude) of that instability when it manifests in the flow field.

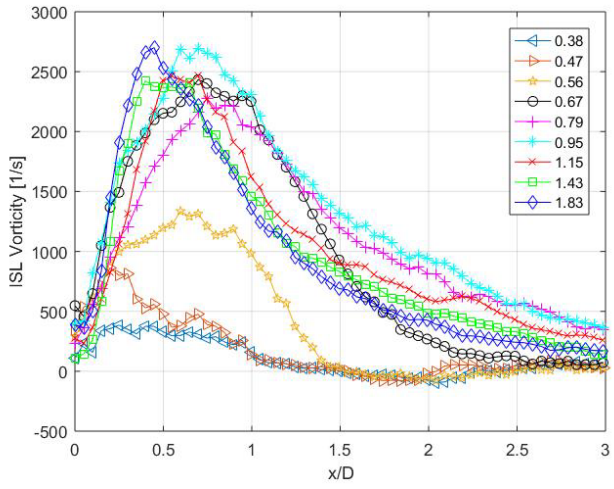


Figure 6. Time-averaged ISL vorticity profile as a function of downstream distance for the 4 in. exit.

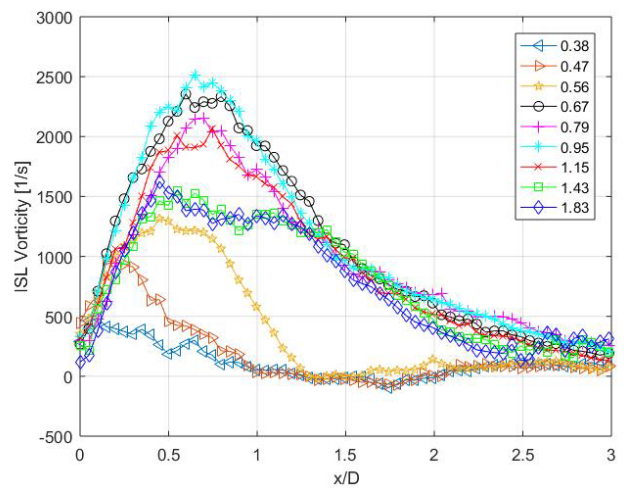


Figure 7. Time-averaged ISL vorticity profile as a function of downstream distance for the 1 in. exit.

In the 4 in. diameter case (Figure 6), the strength of the inner shear layer increases with increasing swirl number. At swirl numbers of S=0.67 and greater, the vorticity profile is similar in both vorticity level and development with downstream distance, which is reflected in the similarity between the vortex breakdown structure in all of these cases. However, in the 1 in. exit boundary case (Figure 7), the ISL strength increases with swirl number until a swirl number of S=0.95, where it peaks. At swirl numbers above S=0.95, the ISL strength decreases; this is likely a result of the deformation of the vortex breakdown bubble and a reduction in recirculation strength that drives the mean shear in the ISL.

Figure 4 shows that the trend in the amplitude of the PVC oscillation with exit boundary diameter bifurcates at this same swirl number, S=0.95. At swirl numbers below this level, the PVC amplitude increases slightly with decreasing exit diameter, but at swirl numbers above this level, the PVC amplitude decreases with decreasing exit diameter. This reduction in PVC strength can be attributed to the reduction in ISL mean shear, which drives the instability through unsteady vortex stretching [19]. If the level of mean shear decreases, the driving force behind coherent structure formation in the PVC is weakened, leading to a lower-amplitude PVC at high swirl numbers and small exit diameter radii.

In the data, the shear layer thickness is not only driven by the changes to the confinement and exit boundary condition, but also the oscillations in the flow (including the PVC). The presence of the PVC will certainly increase the shear layer thickness, as is evidenced in Figure 6 and Figure 7, and so it is difficult to decouple the effect that the base flow (which we can't measure on its own) has on the PVC and the effect that the PVC has on the time-averaged flow (which we can measure). It is intractable to determine the difference between the base flow and the time-averaged flow in experimental data, as we typically use the time-averaged flow as an indicator of the base flow. However, we can infer the effect that the exit boundary condition has shear layer thickness of the base flow in the cases with a PVC by looking at its effect on the cases without a PVC. Comparison of the low swirl number cases in Figure 6 and Figure 7 shows that the shear layer thickens as the diameter of the exit boundary decreases, which is a result of a change in the pressure distribution inside the combustor. As this trend is likely to continue regardless of swirl number, we expect that shear layer thickening of the base flow at high swirl number cases is driving the changes in the PVC dynamics.

## Effect of exit boundary condition on PVC structure

The exit boundary condition has been shown to change the amplitude of the PVC, particularly at high swirl numbers. The structure of the PVC is also altered by changes in swirl number and exit boundary condition, as can be seen in Figure 8. Here, mode shapes from the SPOD are plotted from mode 1 at the PVC frequency. For all cases, the PVC energy is captured almost exclusively in mode 1, and the PVC amplitude is higher than that of motions at other frequencies in mode 1; for this reason, we only show the mode shape from the PVC peak frequency in mode 1.

In the 4 in. case, the PVC structure follows a similar trend to the behavior of the vortex breakdown bubble. As the swirl number increases, the PVC structure shifts upstream, as does the VB bubble. Additionally, the PVC vortices spread radially at a faster rate, a result of the enhanced spreading of the shear layer due to the radial growth of the vortex breakdown bubble and increase in jet spreading due to swirl and confinement. Additionally, the coherent motions in the PVC structure are more "compact" (have a shorter convective wavelength) as the frequency of the PVC increases with swirl number. These trends hold true for the 3 in. and 2 in. exit diameter cases as well.

The PVC structure in the 1 in. exit diameter case, in the left column of Figure 8, has a different progression as the swirl number increases, just as the time-averaged structure of the vortex breakdown bubble did. In this case, the PVC structure moves slightly upstream as swirl number increases, but moreover it loses coherence at the higher swirl numbers. This loss of spatial coherence mimics the reduced amplitude and signal to noise ratio of the peak in the SPOD mode 1 spectrum, indicating that the PVC is being suppressed at this condition. The change in the inner shear layer strength is likely the cause of this degradation of the PVC structure.

#### CONCLUSIONS

In this study, we have experimentally observed the effect that exit boundary condition can have on the structure of a swirling flow and the dynamics of the precessing vortex core, a global instability present in the flow at high swirl numbers. Increasing the swirl number for large exit diameters results in an increase in the strength of the central recirculation zone as well as the amplitude of the PVC oscillations. For the smallest exit boundary diameter (1 in.), however, the recirculation strength and PVC amplitude decreased as a function of swirl number beyond a critical swirl number (S=0.95). In these cases, the PVC lost spatiotemporal coherence with increasing swirl number. Regardless of exit boundary diameter, the PVC frequency increased with swirl number and was relatively insensitive to the exit diameter.

Analysis of the mean shear in the inner shear layer helps to explain why the PVC amplitude trends with swirl number varies so significantly with the exit boundary condition. Linear stability theory indicates that the PVC dynamics are largely governed by the level of swirl and the strength of the mean shear in the inner shear layer. As the structure of the vortex breakdown bubble changed so significantly at the small exit diameters, this change in VB structure reduced the level of mean shear between the annular jet and the fluid in the bubble, reducing the strength of the ISL. In particular, a "jetting" region downstream of the VB bubble emerges at the smallest exit diameters as a result of the strong contraction at the exit of the combustor.

The results of this study could have implications for predicting the dynamics of the precessing vortex core in different combustor geometries. As has been indicated in theoretical predictions in the past, the ISL strength, driven by VB bubble structure, drives the PVC amplitude and coherence. However, in cases where the exit boundary is heavily constricted, as would be

the case with a choked turbine, for example, small changes in the exit boundary condition of the combustor can have significant impacts on the PVC dynamics. As the PVC is one of the most energetic motions in the combustor, these changes to the PVC could have a large impact on combustor operability and thermoacoustic stability limits. Future work will investigate the

coupling of these flow behaviors with changes in flame shape in a reacting case, as the exit boundary condition will likely also drastically impact flame holding, and hence the density gradient that determines flow stability. Further work should also include companion stability analysis to further explore the physical drivers for the differences observed in PVC behaviors.

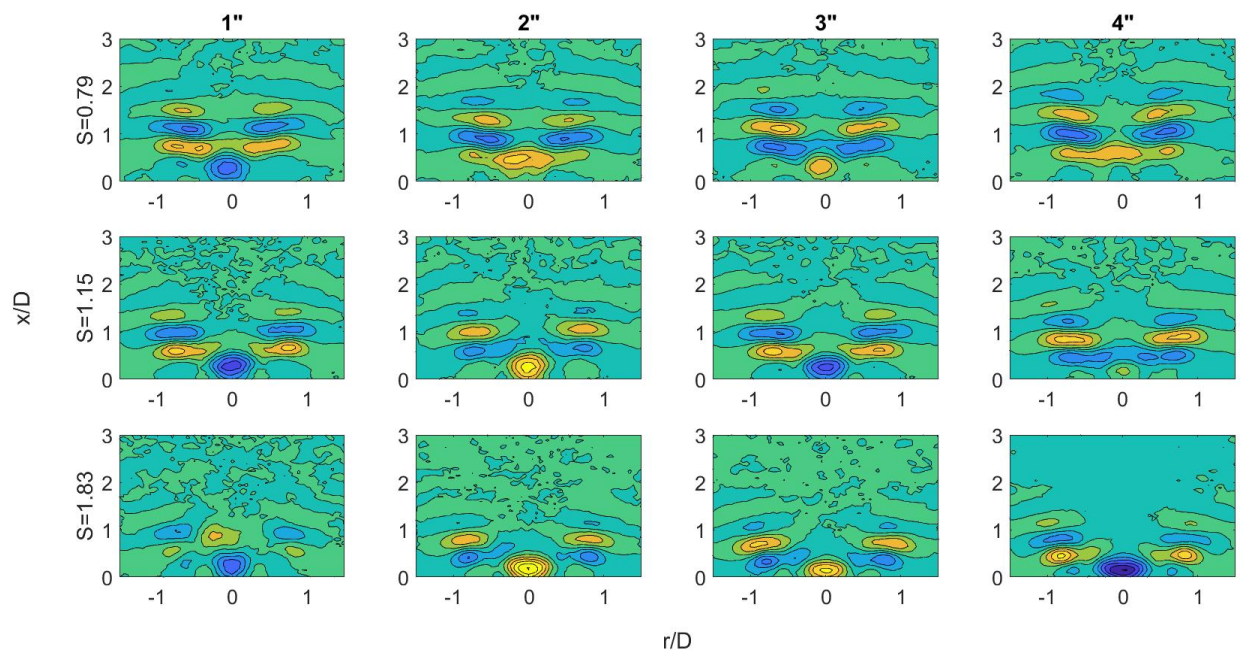


Figure 8. SPOD mode shapes of the PVC at three swirl numbers (rows) and four exit diameters (columns).

#### **ACKNOWLEDGMENTS**

The authors would like to acknowledge Dr. Santosh Hemchandra and Kiran Manoharan from the India Institute of Science – Bangalore for their long-standing collaboration and fruitful feedback on this data. This work was supported by the U.S. National Science Foundation under grant CBET-1749679.

#### **REFERENCES**

- [1] V. McDonell, "Lean Combustion in Gas Turbines," *Lean Combust.*, pp. 147–201, 2016.
- [2] B. T. Zinn and T. Lieuwen, "Combustion Instabilities: Basic Concepts," in *Combustion Instabilities in Gas Turbine Engines: Operational Experience, Fundamental Mechanisms, and Modeling*, T. Lieuwen and V. Yang, Eds. 2005, pp. 3–26.
- [3] S. Ducruix, T. Schuller, D. Durox, and S. Candel, "Combustion Dynamics and Instabilities: Elementary Coupling and Driving Mechanisms," *J. Propuls. Power*, vol. 19, no. 5, pp. 722–734, 2003.
- [4] H. Liang and T. Maxworthy, "An experimental investigation of swirling jets," *J. Fluid Mech.*, vol. 525, pp. 115–159, 2005.
- [5] A. Lefebvre, *Gas Turbine Combustion*. Taylor and Francis, 1999.
- [6] M. Frederick, K. Manoharan, J. Dudash, B. Brubaker, S.

- Hemchandra, and J. O'Connor, "Impact of Precessing Vortex Core Dynamics on Shear Layer Response in a Swirling Jet," *J. Eng. Gas Turbines Power*, vol. 140, no. 6, 2018.
- [7] N. Syred, "A review of oscillation mechanisms and the role of the precessing vortex core (PVC) in swirl combustion systems," *Prog. Energy Combust. Sci.*, vol. 32, no. 2, pp. 93–161, 2006.
- [8] B. Mathews, S. Hansford, and J. O'Connor, "Impact of swirling flow structure on shear layer vorticity fluctuation mechanisms," in *Proceedings of the ASME Turbo Expo*, 2016, vol. 4A–2016.
- [9] D. Darmofal, "The role of vorticity dynamics in vortex breakdown," in 23rd Fluid Dynamics, Plasmadynamics, and Lasers Conference, 1993.
- [10] D. L. Darmofal, R. Khan, E. M. Greitzer, and C. S. Tan, "Vortex core behaviour in confined and unconfined geometries: A quasi-one-dimensional model," *J. Fluid Mech.*, vol. 449, pp. 61–84, Dec. 2001.
- [11] D. L. Darmofal and E. M. Murman, "On the trapped wave nature of axisymmetric vortex breakdown," in 25th AIAA Fluid Dynamics Conference, 1994.
- [12] J. D. Randall and S. Leibovich, "The critical state: a trapped wave model of vortex breakdown," *J. Fluid Mech.*, vol. 58, no. 03, p. 495, May 1973.
- [13] S. Leibovich and K. Stewartson, "A sufficient condition

- for the instability of columnar vortices," *J. Fluid Mech.*, vol. 126, no. 1, p. 335, Jan. 1983.
- [14] T. B. Benjamin, "Theory of the vortex breakdown phenomenon," *J. Fluid Mech.*, vol. 14, no. 4, pp. 593–629, Dec. 1962.
- [15] M. P. Escudier and J. J. Keller, "Recirculation in swirling flows: A manifestation of vortex breakdown," *AIAA J.*, vol. 23, no. 1, pp. 111–116, 1985.
- [16] J. J. Healey, "Inviscid axisymmetric absolute instability of swirling jets," *J. Fluid Mech.*, vol. 613, pp. 1–33, Oct. 2008.
- [17] S. Wang and Z. Rusak, "The dynamics of a swirling flow in a pipe and transition to axisymmetric vortex breakdown," *J. Fluid Mech.*, vol. 340, pp. 177–223, Jun. 1997.
- [18] F. Gallaire and J. M. Chomaz, "Mode selection in swirling jet experiments: A linear stability analysis," *J. Fluid Mech.*, vol. 494, no. 494, pp. 223–253, Nov. 2003.
- [19] K. Manoharan, S. Hansford, J. O'Connor, and S. Hemchandra, "Instability mechanism in a swirl flow combustor: Precession of vortex core and influence of density gradient," in *Proceedings of the ASME Turbo Expo*, 2015, vol. 4A.
- [20] K. Oberleithner *et al.*, "Three-dimensional coherent structures in a swirling jet undergoing vortex breakdown: stability analysis and empirical mode construction," *J. Fluid Mech.*, vol. 679, pp. 383–414, 2011.
- [21] S. Clees, J. Lewalle, M. Frederick, and J. O'Connor, "Vortex core dynamics in a swirling jet near vortex breakdown," in *AIAA Aerospace Sciences Meeting*, 2018, 2018, no. 210059.
- [22] A. Towne, O. T. Schmidt, and T. Colonius, "Spectral proper orthogonal decomposition and its relationship to dynamic mode decomposition and resolvent analysis," *J. Fluid Mech.*, vol. 847, pp. 821–867, 2018.
- [23] A. Karmarkar, M. Frederick, S. Clees, D. Mason, and J. O'Connor, "Role of turbulence in precessing vortex core dynamics," in *ASME Turbo Expo*, 2019.
- [24] I. Chterev *et al.*, "Flame and Flow Topologies in an Annular Swirling Flow," *Combust. Sci. Technol.*, vol. 186, no. 8, pp. 1041–1074, 2014.
- [25] O. Tammisola and M. P. Juniper, "Coherent structures in a swirl injector at Re = 4800 by nonlinear simulations and linear global modes," *J. Fluid Mech.*, vol. 792, pp. 620–657, 2016.